Application of Time-Domain Unsteady Aerodynamics to Rotary-Wing Aeroelasticity

M.A.H. Dinyavari* and P. P. Friedmann†
University of California, Los Angeles, California

This paper presents the methodology for incorporating finite-state, arbitrary motion, time-domain aerodynamics in rotary-wing aeroelastic problems in hover and forward flight. The essential ingredients of a generalized-version Greenberg's theory for time-domain unsteady aerodynamics are presented and incorporated in a coupled nonlinear flap-lag analysis. Aeroelastic stability boundaries for both hover and forward flight are obtained using both arbitrary-motion time-domain aerodynamics and quasisteady aerodynamics. The sensitivity of flap-lag aeroelastic stability boundaries to time-domain, arbitrary-motion unsteady aerodynamics is evaluated by comparing the two sets of results for various blade configurations and flight conditions.

Nomenclature

$[A(\psi,\{q\}_i)]$ = linearized system matrix for ith iteration
$[AAH]$ = aerodynamic stiffness matrix in hover
$[AC1],[AC2]$ = circulatory aerodynamic matrices
$[AD]$ = viscous damping matrix
$[AI1],[AI2],[AI3]$ = inertia matrices
$[ANC1],[ANC2],[ANC3]$ = various noncirculatory aerodynamic matrices
$[AS],[\bar{AS}]$ = structural stiffness matrix $[\bar{\ }] = [\ ] \div (\Omega^2 I_b)$
[AUG] = system matrix for the augmented aerodynamic states
a_i = lift-curve slope
$a_1,a_2 \ldots a_{10}$ = coefficients of the nonlinear terms in circulatory aerodynamic flap moment: $a_{hi} = a_i$ for hover
$\bar{a}bR$ = cross-sectional elastic center (E.C.) offset from midchord
$b_1,b_2 \ldots b_{10}$ = coefficients of the nonlinear terms in circulatory aerodynamic lag moment: $b_{hi} = b_i$ for hover
$bR, b\bar{R}$ = blade semichord: $b\bar{R} = (bR/\ell)$
$C(ik), C(\bar{s})$ = Theodorsen's lift deficiency function and its generalized form
C_T, C_W = rotor thrust and weight coefficients, respectively $(\ )/(\rho_A \pi \Omega^2 R^4)$
$C_\beta, C_\xi, C^*_\beta, C^*_\xi$ = coefficients in perturbational augmented state equations
$e, \bar{e}$ = blade hinge offset from the rotor axis of rotation: $(\bar{e}) = e/\ell$
$F(\bar{X}_{TS1}, \bar{X}_{TS2}, \bar{Q}_{TS}:\psi)$ = time-domain lift deficiency function based on the ¾ radial location: $F = F_b + F_c$
$\{F(\psi,q_i)\}$ = linearized forcing vector for the ith iteration
$F_1(t), F_2(t)$ = functions defined in Eqs. (11a) and (11b)
$\{FC\},\{FNC\}$ = circulatory and noncirculatory aerodynamic forcing vectors, respectively
$\{FI\}$ = vector of inertial loads
g_{sF}, g_{sL} = viscous damping coefficients in flap and lag
$H^+(x^*,t), H^-(x^*,t)$ = source strength on the upper and lower surfaces of the slit
$\Delta h(t)$ = vertical displacement of elastic center of the airfoil, positive downward
i = $\sqrt{-1}$
I_b = blade mass moment of inertia
$K_n(\ )$ = modified Bessel function of the second kind of the order n
$K_{\beta B}, K_{\xi B}$ = root spring stiffness in flap and lag, respectively
L, L_c, L_{nc} = total, circulatory, and noncirculatory components of the lift
$[L(\psi)]$ = linear system matrix in state variable form
ℓ = distance from the pitch bearing to the tip of blade
$[M]$ = total mass matrix including apparent mass
M, M_c, M_{nc} = total, circulatory, and noncirculatory moment components, respectively
M_{ys}, M_{zs} = restoring flap and lag elastic root moments
$\{N_1(q,\psi)\}$ = nonlinear forcing vector
N_b = number of blades
p_u, p_ℓ = pressure on the upper and lower surfaces of the airfoil
$Q(t), Q(s)$ = downwash velocity at the ¾-chord point: $Q(s) = \mathcal{L}[Q(t)]$
$\bar{Q}_{Ts}(\psi)$ = $Q(\psi)$ evaluated at $\bar{x}_0 = \bar{x}_{Ts}$
$\bar{Q}_b(\psi), \bar{Q}_c(\psi)$ = portion of $Q_{TS}(\psi)$ that is dependent on the blade motion and control input only, respectively

Presented as Paper 85-0763 at the AIAA/ASME/ASCE/AHS 26th Structures, Structural Dynamics and Materials Conference, Orlando, FL, April 15-17, 1985; received May 13, 1985; revision received Dec. 3, 1985.

*Postgraduate Research Engineer, Mechanical, Aerospace and Nuclear Engineering Department; presently, Engineer Scientist Specialist, Douglas Aircraft Company, Long Beach, CA. Member AIAA.

†Professor of Engineering and Applied Science, Mechanical, Aerospace and Nuclear Engineering Department. Associate Fellow AIAA.

$Q_{yA}, Q_{zA}; Q_{yI}, Q_{zI}$ = aerodynamic and inertial moments, respectively, at blade root
Q_{yD}, Q_{zD} = viscous damping moments at blade root
q_r, q_θ = radial and tangential disturbance velocities in XZ plane
$R, \bar{R}$ = blade radius: $\bar{R} = (R/\ell)$
R_c = elastic coupling parameter
$s, \bar{s}$ = Laplace transform variable: $\bar{s} = (sbR/U_{T0})$
t, t', τ = time
$U_T(t), U_p(t)$ = freestream velocity in x^* and negative z^* directions, respectively: $U_T(t) = U_{T0} + \Delta U_T(t)$; $U_p(t) = U_{P0} + \Delta U_p(t)$
$\bar{U}_{TS0}$ = constant portion of $\bar{U}_y''$ evaluated at the typical section: $\bar{U}_y'' = \bar{x}_{TS0} + \bar{e}$
U_x'', U_y'', U_z'' = components of blade cross-section elastic center velocity vector in the deformed blade coordinate system $(\bar{\ }) = (\ )/(\Omega\ell)$
$W_a(x^*, \tau), W_a(\bar{\phi}, \tau)$ = upwash velocity over the airfoil
$W_{am}(\tau)$ = Fourier coefficients of W_a
$X_0^*(\tau)$ = location of trailing edge of the wake behind the reference airfoil at time $t = \tau$
$X_1(t), X_2(t)$ = augmented aerodynamic state variables
$\bar{X}_{TS1}(\psi), \bar{X}_{TS2}(\psi)$ = nondimensional X_1 and X_2 for the typical section
$\bar{X}_{1c}(\psi), \bar{X}_{2c}(\psi), \bar{X}_{1b}(\psi), \bar{X}_{2b}(\psi)$ = portions of $\bar{X}_{TS1}$ and $\bar{X}_{TS2}$ due to $\bar{Q}_c$ and $\bar{Q}_b$, respectively
x_A, x_I = aerodynamic center and center-of-gravity offsets from the elastic center: $(\bar{\ }) = (\ )/bR$
$\{Z(\psi)\}$ = linear forcing vector for the system in state variable form
$\alpha(t), \alpha_0, \Delta\alpha(t)$ = time-variant angle of incidence of the airfoil at the elastic center, measured clockwise from the horizontal x^* axis: $\alpha(t) = \alpha_0 + \Delta\alpha(t)$
β, ζ = blade flap and lead-lag angles, respectively
β_p = blade precone
γ = Lock number
$\gamma_t(t')$ = trailing-edge vortex strength shed at time $t = t'$
$\gamma_W(\xi^*, \tau)$ = wake vortex strength distribution at time $t = \tau$, positive clockwise
ζ_k = real part of the kth eigenvlaue or characteristic exponent
θ_G = total geometric pitch angle about feathering axis
$\theta_0, \theta_{1c}, \theta_{1s}$ = collective pitch, lateral, and longitudinal cyclic pitch angles, respectively
λ = inflow ratio
λ_k = eigenvalues or characteristic exponents
μ = advance ratio
$\xi^*(t', \tau)$ = location of the vortex that was shed at time $t = t'$ observed at time $t = \tau$
ρ_A = density of air
σ = rotor solidity ratio $(2bN_b/\pi)$
ϕ' = disturbance velocity potential
ψ = azimuth angle of blade
Ω = rotor speed of rotation
ω_k = imaginary part of kth eigenvalue or characteristic exponent
$\bar{\omega}_{F1}, \bar{\omega}_{L1}$ = fundamental rotating flap and lead-lag frequencies nondimensional with respect to Ω
∇^2 = Laplacian operator
$(\dot{\ })$ = $\partial/\partial t$
$(*)$ = $\partial/\partial\psi$

I. Introduction and Problem Statement

THE unsteady aerodynamic environment encountered in helicopter rotors is complicated. An accurate evaluation of the aerodynamic loads is a key ingredient in the analytical prediction of the aeroelastic behavior of helicopter rotor blades. The most advanced aerodynamic analyses presently available for below-stall condition are "free-wake" analyses. Lifting-surface-type theories are required to model blade/vortex interaction and three-dimensional tip effects. Furthermore, computational fluid mechanics are required to capture nonlinear transonic effects at the blade tip. Due to the large amounts of computer time required for these more sophisticated aerodynamic theories, many rotary-wing aeroelastic analyses use unsteady or quasisteady two-dimensional aerodynamic theories,[1,2] so as to determine fundamental trends in blade behavior.

Until recently, all unsteady aerodynamic theories used in rotary-wing applications were based on the assumption of simple harmonic motion. A major shortcoming of these theories is that they are suitable only for determining aeroelastic stability boundaries and are not capable of predicting damping levels at subcritical conditions. More importantly, due to the periodic coefficients present in the dynamic equations of equilibrium in forward flight, the frequency-domain unsteady aerodynamic theories are not suitable for forward flight applications. Therefore many analyses dealing with forward flight use quasisteady aerodynamics.[1,2]

In Ref. 3, three incompressible, finite-time, arbitrary-motion airfoil theories, suitable for coupled flap-lag-torsional aeroelastic analysis of rotary blades are described. These theories include the generalized versions of Greenberg's[4] theory and Loewy's,[5] as well as a generalized cascade-wake theory.

An important feature of these theories is their ability to simulate arbitrary motions (e.g., decaying or growing harmonic oscillations); thus, these theories are valid for subcritical (i.e., below flutter margin) as well as supercritical conditions. These theories are useful for the development of augmented-state (finite-state) aeroelastic models for rotary-wing problems. The role of augmented states is to convey information regarding the unsteady wake. The system of governing equations associated with the augmented states has to be appended to the aeroelastic equations of motion and solved simultaneously. Furthermore, finite-state, arbitrary-motion aerodynamic theories, in the time domain, are compatible with the blade dynamic equations of motion in forward flight that contain periodic coefficients.[1,2]

The primary objectives of this study are: 1) to present a brief derivation of the generalized Greenberg theory that is applicable to both hover and forward flight, 2) to illustrate the general methodology for incorporating finite-state, arbitrary-motion time-domain aerodynamics in a rotary-wing aeroelastic problem in hover and forward flight, and 3) to develop a mathematical solution technique capable of dealing with an aeroelastic problem in which arbitrary-motion unsteady aerodynamics are combined with nonlinear equations of blade equilibrium having period coefficients. Since this is the first application in the literature of the field of such aerodynamics to a rotary-wing aeroelastic problem, the relatively simple flap-lag aeroelastic problem in hover and forward flight has been selected as an illustrative example. This coupled flap-lag aeroelastic problem is treated by using an offset-hinged, spring-restrained model of the blade, where the root springs simulate blade flexibility in flap and lag. This model was first used by Ormiston and Hodges[6] to treat the linear flap-lag problems in hover and was subsequently

used by Peters to represent the flap-lag problem in forward flight.[7,8] This model was also found to be a useful means for illustrating the influence of dynamic inflow on rotary-wing aeroelasticity,[9] which represents a low-frequency approximation to arbitrary-motion type of unsteady aerodynamics.[8,10]

In this study the generalized Greenberg-type time-domain unsteady aerodynamics are incorporated in the coupled flap-lag aeroelastic problem.[1,2] The nonlinearities in the problem are geometrical, due to moderate blade deflections, and the blade dynamic equations of equilibrium have periodic coefficients due to forward flight. Aeroelastic stability boundaries for both hover and forward flight are obtained using arbitrary-motion time-domain aerodynamics as well as quasisteady aerodynamics. The sensitivity of the stability boundaries to the type of aerodynamics used is determined by comparing the two sets of results for various blade configurations and flight conditions.

One of the main accomplishments of this study is the development of mathematical solution techniques for dealing with a problem that combines arbitrary-motion unsteady aerodynamics with nonlinear dynamic equations of blade equilibrium having periodic coefficients. These methods are applicable to more complicated rotary-wing aeroelastic problems, such as the coupled flap-lag-torsional problem in forward flight, the coupled rotor/fuselage aeromechanical problem in forward flight,[1,2] or problems that combine rotor dynamics and active controls.

II. Generalized Greenberg Theory for Arbitrary Motion

A generalization of Greenberg's theory for arbitrary motion is outlined in Ref. 3. A more complete derivation of this theory is presented here.

In this study, an approach similar to that used by Edwards[11] to generalize Theodorsen's theory is applied to Greenberg's theory. Expressions for the calculation of unsteady lift and moment of an airfoil undergoing arbitrary plunge and pitch motion about a steady pitch angle in the presence of time-varying oncoming velocity and variable inflow are obtained. The aerodynamic loads are derived in Laplace, frequency, and time domains. The time-varying oncoming velocity allows for modeling streamwise blade motion as well as time variation of velocity due to forward flight. As with Greenberg's theory, the flow is assumed to be two-dimensional, incompressible, and irrotational. In addition, the disturbance due to airfoil motion and the free-stream fluctuations are assumed to be small.

The geometry of the airfoil dynamics is shown in Fig. 1. The upwash velocity distribution required to satisfy tangent flow condition over the airfoil is given by

$$W_a(\bar{\theta},t) = -\{[U_{T0}+\Delta U_{T0}(t)][\alpha_0+\Delta\alpha(t)] + bR(\cos\bar{\theta}-\bar{a})\Delta\dot{\alpha}(t) + [\Delta\dot{h}(t)-U_{p0}-\Delta U_p(t)]\} = W_{a0}(t)+W_{a1}(t)\cos\bar{\theta} \tag{1a}$$

where

$$\bar{\theta}=\cos^{-1}(x^*/bR) \tag{1b}$$

The disturbance potential function is governed by the Laplace equation

$$\nabla^2\phi' = 0 \tag{2}$$

The tangent flow boundary condition is satisfied by distributing source-and-sink pair solutions over the airfoil

$$H^+(x^*,z^*=0^+,t) = 2W_a(x^*,t)$$
$$H^-(x^*,z^*=0^-,t) = -2W_a(x^*,t) \tag{3}$$

It is shown in Ref. 12 that the noncirculatory disturbance potential for the points on the upper surface of the airfoil is given by

$$\phi'_{nc}(\bar{\theta},z^*=0,t) = -(bR/2)[2W_{a0}(t)\sin\bar{\theta} + 1/2W_{a1}\sin(2\bar{\theta})] \tag{4}$$

Using the unsteady linearized Bernoulli's equation for the pressure, the noncirculatory lift and moment acting at the elastic center of the airfoil can be written as

$$L_{nc}(t) = \rho_A\pi(bR)^2\{\Delta\ddot{h}(t)+U_T(t)\Delta\dot{\alpha}(t) + \dot{U}_T(t)[\alpha_0+\Delta\alpha(t)]-\dot{U}_p(t)-(\bar{a}bR)\Delta\ddot{\alpha}(t)\} \tag{5a}$$

and

$$M_{nc}(t) = \underline{\rho_A\pi(bR)^2U_T(t)Q(t)} + \rho_A\pi(bR)^3\{(\bar{a}-1/2)U_T(t)\Delta\dot{\alpha}(t)+\bar{a}[\Delta\ddot{h}-\dot{U}_p(t)] + \bar{a}\dot{U}_T(t)[\alpha_0+\Delta\alpha(t)]-bR(1/8+\bar{a}^2)\Delta\ddot{\alpha}(t)\} \tag{5b}$$

where

$$Q(t) = -[W_{a0}(t)+1/2W_{a1}(t)] = U_T(t)[\alpha_0+\Delta\alpha(t)] + [\Delta\dot{h}(t)-U_p(t)]+bR(1/2-\bar{a})\Delta\dot{\alpha}(t) \tag{5c}$$

The underlined term in the expression for M_{nc} cancels out with circulatory load terms; hence, it is not expanded. The above solution does not satisfy the Kutta condition at the trailing edge. To satisfy the Kutta condition, a circulatory flow must be added

$$q_{\theta c}(\bar{\theta}=0,\tau)+q_{\theta nc}(\bar{\theta}=0,\tau)=0 \tag{6}$$

A pattern of vortices is placed on the segment of the wake that has been influenced by the shed vortices since the beginning of the motion (Fig. 2). In addition, bound vortices are placed on the airfoil so that the normal velocity on the airfoil due to circulatory flow is zero at every instant of time; hence, the tangent-flow boundary condition already satisfied by noncirculatory flow remains valid. The imposition of the Kutta condition yields a singular integral equation over the finite wake length of the shed vortices, in terms of wake vortex strength:

$$-\frac{1}{2\pi bR}\int_{bR}^{X_0^*(\tau)}\sqrt{\frac{\xi^*+bR}{\xi^*-bR}}\gamma_W(\xi^*,\tau)\,d\xi^* = Q(\tau) \tag{7}$$

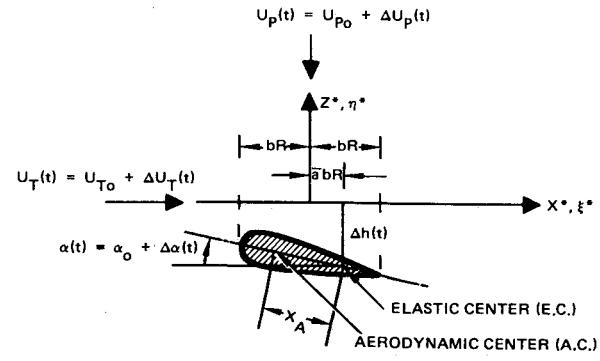

Fig. 1 Geometry of motion of a typical airfoil.

The circulatory lift and moment in terms of the wake vortex distribution are given by

$$L_c(\tau) = -\rho_A U_T(\tau) \int_{bR}^{X_0^*(\tau)} \frac{\xi^*}{\sqrt{[\xi^{*2} - (bR)^2]}} \gamma_W(\xi^*, \tau) d\xi^* \quad (8a)$$

$$M_c(\tau) = \rho_A (bR) U_T(\tau) \int_{bR}^{X_0^*(\tau)} \left[\frac{1}{2} \sqrt{\frac{\xi^* + bR}{\xi^* - bR}} - \left(\bar{a} + \frac{1}{2}\right) \frac{\xi^*}{\sqrt{\xi^{*2} - (bR)^2}} \right] \gamma_W(\xi^*, \tau) d\xi^* \quad (8b)$$

The condition of zero pressure discontinuity across the wake requires the vortices shed at the trailing edge to travel downstream with the freestream velocity

$$\frac{\partial \xi^*}{\partial t'} = -U_T(t') \quad (9a)$$

where ξ^* is the position of a vortex shed at time t' as a function of time τ and can be expressed in terms of the oncoming velocity as

$$\xi^*(t', \tau) = bR + \int_{t'}^{\tau} U_T(t) dt \quad (9b)$$

Using the exact downstream velocity of shed vortices, but assuming a mean value for their position, yields

$$\xi^*(t', t) = bR + U_{T0}(\tau - t') \quad (9c)$$

A change of variable from the position along the wake to the time variable can be introduced. Using this change of variable, the integral equation of downwash [Eq. (7)] and the circulatory lift and moment expressions [Eqs. (8)] can be transformed into convolution form:

$$\frac{-1}{(2\pi bR)} \int_0^{\tau} [F_1(\tau - t')] [U_T(t') \gamma_t(t')] dt' = Q(\tau) \quad (10a)$$

$$\frac{L_c(\tau)}{\rho_A U_T(t)} = -\int_0^{\tau} [F_2(\tau - t')] [U_T(t') \gamma_t(t')] dt' \quad (10b)$$

$$\frac{M_c(\tau)}{\rho_A (bR) U_T(t)} = \int_0^{\tau} [1/2 F_1(\tau - t') - (\bar{a} + 1/2) F_2(\tau - t')] \times (U_T(t') \gamma_t(t')] dt' \quad (10c)$$

where

$$F_1(t) = \sqrt{[t + (2bR/U_{T0})]/t} \quad (11a)$$

$$F_2(t) = [t + bR/U_{T0})]/\sqrt{t^2 + (2bR/U_{T0})t} \quad (11b)$$

Application of Laplace transformation to the integral equation of downwash and the circulatory loads in the convolution form allows the elimination of the unknown trailing-edge vortex strength, and the solution for the circulatory lift and moment in the Laplace domain

$$\mathcal{L}\left[\frac{L_c(t)}{\rho_A U_T(t)}\right] = (2\pi)(bR) C(\bar{s}) \mathcal{L}[Q(t)] \quad (12a)$$

$$\mathcal{L}\left[\frac{M_c(t)}{\rho_A (bR) U_T(t)}\right] = (2\pi)(bR)\{-1/2 + (\bar{a} + 1/2) C(\bar{s})\} \times \mathcal{L}[Q(t)] \quad (12b)$$

where

$$C(\bar{s}) = \frac{K_1(\bar{s})}{K_1(\bar{s}) + K_0(\bar{s})}, \qquad \bar{s} = \frac{sbR}{U_{T0}} \quad (12c)$$

From Eqs. (12) it is evident that the lift deficiency function $C(\bar{s})$, identical to the generalized Theodorsen's lift deficiency function, acts as a Laplace domain operator between the ¾-chord downwash velocity and the circulatory loads divided by the time-varying oncoming velocity.

A second-order Pade approximant, i.e., ratio of two quadratic polynomials, for the generalized Theodorsen's lift deficiency function $C(\bar{s})$ is used to obtain the time-domain loads.[3]

$$C(\bar{s}) = \frac{0.5(\bar{s})^2 + 0.2808(\bar{s}) + 0.01365}{(\bar{s})^2 + 0.3455(\bar{s}) + 0.01365} \quad (13)$$

Using Eq. (13) a second-order finite-state time-domain representation of the circulatory loads is obtained in terms of the airfoil degrees of freedom and their time derivatives and two additional augmented state variables.

$$L_c(t) = 2\pi\rho_A (bR) U_T(t) [0.00685 (U_{T0}/bR)^2 X_1(t) + 0.10805 (U_{T0}/bR) X_2(t)] + \pi\rho_A (bR) U_T(t) Q(t) \quad (14a)$$

$$M_c(t) = (bR)(\bar{a} + 1/2) L_c(t) \quad (14b)$$

The augmented state variables X_1 and X_2 are governed by a system of ordinary differential equations that is associated with the ¾-chord downwash velocity $Q(t)$

$$\begin{Bmatrix} \dot{X}_1(t) \\ \dot{X}_2(t) \end{Bmatrix} = \begin{bmatrix} 0 & 1 \\ -0.01365 (U_{T0}/bR)^2 & -0.3455 (U_{T0}/bR) \end{bmatrix} \times \begin{Bmatrix} X_1(t) \\ X_2(t) \end{Bmatrix} + \begin{Bmatrix} 0 \\ Q(t) \end{Bmatrix} \quad (15)$$

It should be noted that the portion of the circulatory moment that is canceled out by the underlined term in Eq. (5b) has been left out.

The second-order, finite-state, approximate time-domain representation of the unsteady loads is in a form compatible with blade equations of motion in hover or forward flight. The unsteady loads are in terms of two additional augmented states, which convey information regarding the unsteady wake history. The augmented states are governed by a first-order linear system, of size 2, which is forced by the airfoil ¾-chord-point downwash velocity. This aerodynamic theory represents a good approximation for both low- and high-frequency regimes of blade motion.

A final comment regarding the accuracy of the assumptions is made. As with Greenberg's theory, the generalized theory presented here utilizes the mean freestream velocity to define the position of the vortices in the airfoil wake; however, it uses the exact time-varying velocity at which the wake vortices travel downstream. A close examination of the

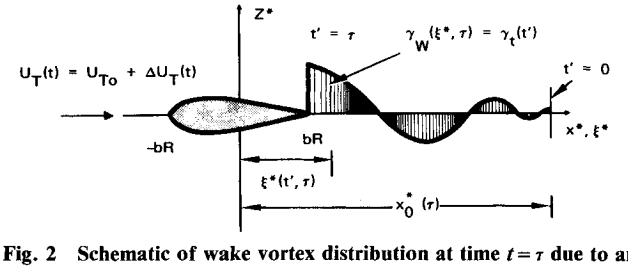

Fig. 2 Schematic of wake vortex distribution at time $t = \tau$ due to an arbitrary finite-time airfoil motion between $t = 0$ and $t = \tau$.

Biot-Savart law and Bernoulli's equation reveals that the unsteady airloads are much more sensitive to the velocity of the wake vortices than their position. This is due to the fact that the position of vortices appears in the denominator terms whereas the velocity of vortices occurs in the numerator terms. Furthermore, in foward flight the dominant freestream variation is at one per rotor revolution for which the reduced frequency is low. However, the generalized Greenberg theory is aimed primarily at capturing the effects associated with higher frequencies where unsteady aerodynamic effects could be important. The amplitude of the streamwise variations tends to be much lower at these higher frequencies.

III. Aeroelastic Equations of Motion and Their Solution

Blade Equations of Motion

The blade equations of motion, for an offset-hinged, spring-restrained hingeless blade model in hover and forward flight, were derived in Ref. 13. The geometry of the problem is shown in Fig. 3. In Ref. 13 three orthogonal springs representing flap, lag, and torsion were used. However, for the present case, the torsional spring is assumed to be rigid and the equations are reduced to coupled flap-lag equations of motion. The most important ingredient in the equations is the assumption of moderate blade deflections, which introduces geometrically nonlinear effects.[1,2,12,13]

The dynamic equations of motion for the blade are obtained from a Newtonian approach by combinging the structural operator with inertial, aerodyanmic, and structural damping and using d'Alembert's principle. The aerodynamic and inertia operators are obtained by integrating the distributed loads per unit length of the blade to obtain the corresponding blade root moments.

$$M_{ys}+Q_{yI}+Q_{yD}+Q_{yA}=0$$
$$M_{zs}+Q_{zI}+Q_{zD}+Q_{zA}=0 \tag{16}$$

The structural, inertia, and damping moments can be written symbolically as

$$\begin{Bmatrix} M_{ys} \\ M_{zs} \end{Bmatrix} = (\Omega^2 I_b)\,[\overline{AS}] \begin{Bmatrix} \beta \\ \zeta \end{Bmatrix} \tag{17}$$

$$\begin{Bmatrix} Q_{yI} \\ Q_{zI} \end{Bmatrix} = (\Omega^2 I_b) \left\langle [AI1] \begin{Bmatrix} \beta \\ \zeta \end{Bmatrix} + [AI2] \begin{Bmatrix} \overset{*}{\beta} \\ \overset{*}{\zeta} \end{Bmatrix} + [AI3] \begin{Bmatrix} \overset{**}{\beta} \\ \overset{**}{\zeta} \end{Bmatrix} + \begin{Bmatrix} 2\beta\overset{*}{\zeta} \\ 2\beta\overset{*}{\beta} \end{Bmatrix} + \begin{Bmatrix} FI(1) \\ FI(2) \end{Bmatrix} \right\rangle \tag{18}$$

$$\begin{Bmatrix} Q_{yD} \\ Q_{zD} \end{Bmatrix} = (\Omega^2 I_b)\,[AD] \begin{Bmatrix} \overset{*}{\beta} \\ \overset{*}{\zeta} \end{Bmatrix} \tag{19}$$

where the detailed expressions for various matrices in Eqs. (17-19) are given in Ref. 12.

Incorporation of Finite-State Time-Domain Aerodynamic Loads in the Blade Equations of Motion

The generalized aerodynamic loads consist of two parts: 1) circulatory loads that involve the augmented states as well as the blade dynamics, and 2) noncirculatory loads that involve only the blade dynamics. The loads per unit span of the blade, in the underformed coordinate system, obtained from the application of the two-dimensional arbitrary-motion airfoil theory were presented in Refs. 3 and 12. To incorporate these loads into the flap-lag analysis used in this paper, a transformation from the deformed coordinate system to the underformed coordinate sytem[12] is required. In this process the identification of the various velocity components in the blade-fixed, deformed coordinate system is needed. To formulate the aeroelastic equations of motion, the integrals of the aerodynamic loads over the span of the blade have to be evaluated. The task of obtaining the appropriate integrals of the noncirculatory loads over the blade, although algebraically involved, does not pose any difficulty. However, treatment of the integration of the circulatory loads over the blade involves special considerations due to the augmented states.

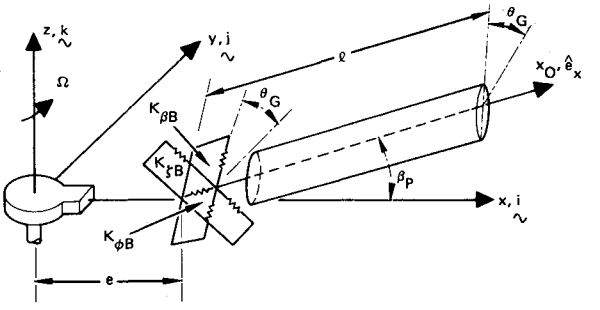

Fig. 3 Geometry of offset-hinged, spring-restrained, rigid-blade model of a hingeless rotor.

The circulatory lift and moment of the finite-state, time-domain generalized Greenberg's theory, Eqs. (14a) and (14b), can be written in terms of their quasisteady value multiplied by a time-domain lift deficiency function as follows:

$$\bar{L}_c = \left[\frac{L_c}{\rho_A a_i (bR)(\Omega\ell)^2}\right] = [1/2 + F(\psi)]\,\bar{U}_y''\bar{Q} \tag{20}$$

$$\bar{M}_c = \left[\frac{M_c}{\rho_A a_i (bR)^2(\Omega\ell)^2}\right] = \bar{x}_A\,[1/2 + F(\psi)]\,\bar{U}_y''\bar{Q} \tag{21}$$

where

$$\bar{U}_y'' = [(\bar{x}_0 + \bar{e}) + \mu\bar{R}\sin\psi + \bar{x}_0\overset{*}{\zeta} + \mu\bar{R}\cos\psi\zeta]$$
$$\bar{U}_z'' = [\bar{R}\lambda + \bar{x}_0\overset{*}{\beta} + (\mu\bar{R}\cos\psi + \bar{x}_0\zeta)(\beta_p + \beta)]$$
$$\bar{Q} = [\bar{U}_y''\theta_G - \bar{U}_z'' + b\bar{R}(1-\bar{x}_A)\overset{*}{\theta}_G] \tag{22}$$

and $F(\psi)$ is the lift deficiency function in the time domain, which is a function of the augmented states of the blade section.

Each cross section along the blade span introduces its own set of augmented states. To integrate the loads, a finite number of stations along the blade is selected. From these stations a typical section along the blade is identified that represents the unsteady aerodynamic effects in an average manner. A preliminary study using frequency-domain unsteady aerodynamics for a centrally hinged, spring-restrained, rigid blade having only a flap degree of freedom was performed.[14] This study showed that the ¾-span location represents a good average for the phase and amplitude of the lift deficiency function for the entire blade. Therefore a ¾-span location was selected as the typical section. Using this assumption, $F(\psi)$ becomes only a temporal function, which is valid for the entire blade span.The expression for $F(\psi)$ in terms of the augmented states corresponding to the typical section is given by

$$F(\bar{X}_{TS1}, \bar{X}_{TS2}, \bar{Q}_{TS}:\psi) = \frac{\left[0.006825\left(\frac{\bar{U}_{TS0}}{b\bar{R}}\right)^2\right]\bar{X}_{TS1} + \left[0.10805\left(\frac{\bar{U}_{TS0}}{b\bar{R}}\right)\right]\bar{X}_{TS2}}{\bar{Q}_{TS}} \tag{23}$$

where

$$\bar{Q}_{TS} = \bar{Q} \text{ evaluated at } \bar{x}_0 = \bar{x}_{TS}$$

$$\bar{U}_{TS0} = \bar{x}_{TS} + \bar{e}$$

and

$$\begin{Bmatrix} \overset{*}{\bar{X}}_{TS1} \\ \overset{*}{\bar{X}}_{TS2} \end{Bmatrix} = \left[\begin{array}{c|c} \text{AUG}(1,1) & \text{AUG}(1,2) \\ \hline \text{AUG}(2,1) & \text{AUG}(2,2) \end{array}\right] \begin{Bmatrix} \bar{X}_{TS1} \\ \bar{X}_{TS2} \end{Bmatrix} + \begin{Bmatrix} 0 \\ \bar{Q}_{TS} \end{Bmatrix} \tag{24a}$$

$$\text{AUG}(1,1) = 0, \quad \text{AUG}(1,2) = 1$$

$$\text{AUG}(2,1) = -0.01365[\bar{U}_{TS0}/b\bar{R}]^2$$

$$\text{AUG}(2,2) = -0.3455[\bar{U}_{TS0}/b\bar{R}] \tag{24b}$$

Using Eqs. (20-22) for the two-dimensional airloads and accounting for unsteady parasite drag force, the aerodynamic root moments become[12]

$$\left(\frac{1}{\Omega^2 I_b}\right)\begin{Bmatrix} Q_{yA} \\ Q_{zA} \end{Bmatrix} = [1/2 + F(\psi)]\left\langle [AC1]\begin{Bmatrix} \beta \\ \zeta \end{Bmatrix} + [AC2]\begin{Bmatrix} \overset{*}{\beta} \\ \overset{*}{\zeta} \end{Bmatrix}\right.$$

$$+ \{[a_1\beta^2 + a_2\zeta^2 + a_3\beta\zeta + a_4\beta\overset{*}{\zeta} + a_5\overset{*}{\beta}\zeta + a_6\overset{*}{\beta}\overset{*}{\zeta} + a_7\overset{*}{\beta}^2 + a_8\overset{*}{\zeta}^2$$

$$+ a_9\beta\overset{*}{\beta} + a_{10}\zeta\overset{*}{\zeta}]/[b_1\beta^2 + b_2\zeta^2 + b_3\beta\zeta + b_4\beta\overset{*}{\zeta} + b_5\overset{*}{\beta}\zeta$$

$$+ b_6\overset{*}{\beta}\overset{*}{\zeta} + b_7\overset{*}{\beta}^2 + b_8\overset{*}{\zeta}^2 + b_9\beta\overset{*}{\beta} + b_{10}\zeta\overset{*}{\zeta}]\}$$

$$\left. + \begin{Bmatrix} FC(1) \\ FC(2) \end{Bmatrix}\right\rangle + [ANC1]\begin{Bmatrix} \beta \\ \zeta \end{Bmatrix} + [ANC2]\begin{Bmatrix} \overset{*}{\beta} \\ \overset{*}{\zeta} \end{Bmatrix}$$

$$+ [ANC3]\begin{Bmatrix} \overset{**}{\beta} \\ \overset{**}{\zeta} \end{Bmatrix} + \begin{Bmatrix} FNC(1) \\ FNC(2) \end{Bmatrix} \tag{25}$$

The detailed expressions for the various matrices and coefficients used in Eq. (25) can be found in Ref. 12.

Method of Solution in Hover

The aeroelastic problem in hover is solved as follows:

1) For uniform inflow and a given collective pitch angle, the nonlinear static equilibrium position of the blade is evaluated using a Newton-Raphson iterative scheme.[1,2] The static equilibrium position of the blade is denoted by β_e and ζ_e, where the subscript e denotes the equilibrium value.

2) The dynamic equations of motion are linearized about the equilibrium position by writing perturbation equations and neglecting the second-order terms in the perturbation quantities.[1,2] The linearized equations are rewritten in first-order state variable form. The first-order system is a 4×4 system for quasisteady aerodynamics, and a 6×6 system for the case with finite-state time-domain aerodynamics. The first-order system for the case with finite-state time-domain aerodynamics has the following form:

$$\{\Delta\overset{*}{q}\}_i = [A(q_i)]_i\{\Delta q\}_i \tag{26}$$

where Δq_j, $j = 1, 6$ are

$$\Delta q_1 = \Delta\beta, \quad \Delta q_2 = \Delta\zeta, \quad \Delta q_3 = \Delta\bar{X}_{TS1}$$

$$\Delta q_4 = \Delta\overset{*}{\beta}, \quad \Delta q_5 = \Delta\overset{*}{\zeta}, \quad \Delta q_6 = \Delta\bar{X}_{TS2} \tag{27}$$

3) An eigenanalysis of the linearized system is carried out. From the eigenvalues $\lambda_k = \zeta_k + i\omega_k$, the stability of the system is determined; when $\zeta_k > 0$, the system is unstable.

Method of Solution for Forward Flight

For the case of forward flight, the equations of motion are ordinary nonlinear equations with periodic coefficients. The problem is further complicated by the fact that in forward flight the aeroelastic stability and response of the isolated blade is coupled with the overall flight condition of the helicopter.[1,2,15,16] Therefore, the first step in the solution is the evaluation of the trim state of the helicopter. In this paper a propulsive trim procedure[15,16] is used that simulates actual forward flight conditions, including the effects of reversed flow and flap response. For a given value of the advance ratio μ, and the nondimensional weight coefficient C_W, the trim quantities are calculated by enforcing horizontal and vertical force equilibrium combined with the requirement of zero pitch and rolling moments about the helicopter center of gravity. After the trim state is obtained, the aeroelastic stability problem is solved in two stages.

The first stage of the solution consists of the calculation of the nonlinear periodic equilibrium position of the blade using quasilinearization.[16] An important ingredient in the calculation of the time-dependent equilibrium position is the treatment of the time-domain lift deficiency function $F(\psi)$, which is a nonlinear function of the ¾-chord downwash velocity and has an implicit form.

The nondimensional ¾-downwash velocity at the typical section can be decomposed into two portions: 1) a portion that depends only on the collective and cyclic pitch inputs and the inflow velocity Q_c and 2) a portion that is a function of the motion of the blade as well as the total pitch angle $\bar{Q}_b$:

$$\bar{Q}_{TS} = \bar{Q}_c + \bar{Q}_b \tag{28}$$

Since the governing equations for the augmented states are linear in terms of the ¾-chord point downwash velocity, the augmented states can also be expressed in a similar manner

$$\bar{X}_{TS1} = \bar{X}_{1c} + \bar{X}_{1b}$$

$$\bar{X}_{TS2} = \bar{X}_{2c} + \bar{X}_{2b} \tag{29}$$

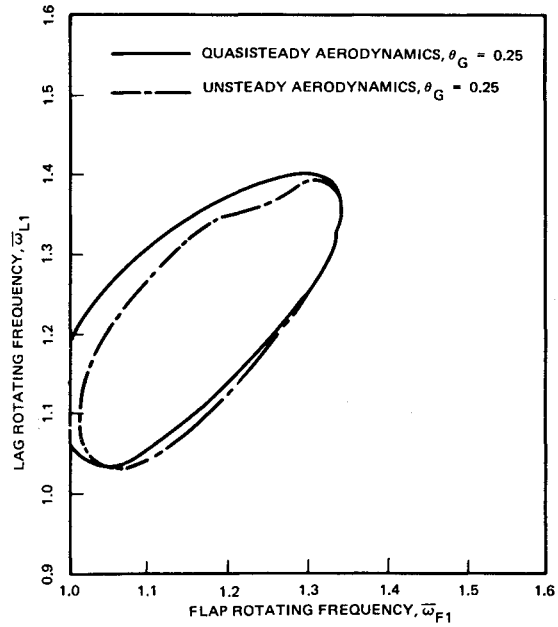

Fig. 4 Comparison of stability boundaries calculated using quasisteady and unsteady aerodynamics for $\theta_G = 0.25$. ($R_c = 0.0$, $\gamma = 5.0$, $\sigma = 0.05$, $b = 0.01964$, $x_A = x_I = e = \beta_p = 0.0$, no apparent mass.)

where $\bar{X}_{1c}$ and $\bar{X}_{2c}$ are due to $\bar{Q}_c$ while $\bar{X}_{1b}$ and $\bar{X}_{2b}$ are associated with $\bar{Q}_b$. Thus the time-domain lift deficiency function $F(\psi)$ can be written as a combination of two parts:

$$F(\bar{X}_{TS1},\bar{X}_{TS2},\bar{Q}_{TS}:\psi) = F_c(\bar{X}_{1c},\bar{X}_{2c},\bar{Q}_c:\psi) + F_b(\bar{X}_{1b},\bar{X}_{2b},\bar{Q}_b:\psi) \tag{30}$$

It was shown in Ref. 12 that $\bar{X}_{1c}$, $\bar{X}_{2c}$, and F_c are independent of blade motion, whereas $\bar{X}_{1b}$, $\bar{X}_{2b}$, and F_b are nonlinear functions of the blade motion. The exact closed-form solutions for $\bar{X}_{1c}$, $\bar{X}_{2c}$, and $F_c(\psi;Q_c)$ are given in Ref. 12.

Using this decomposition for $F(\psi)$, the linear and nonlinear portions of the equations of the motion in forward flight can be identified

$$\{\overset{*}{q}\} = [L(\psi)]\{q\} + \{Z(\psi)\} + \{N_1(q,\psi)\} \tag{31}$$

where

$$\{q\}^T = [\beta,\zeta,\bar{X}_{1b},\overset{*}{\beta},\overset{*}{\zeta},\bar{X}_{2b}]$$

It should be noted that the nonlinear vector $\{N_1\}$ is only a function of state vector $\{q\}$ and is not a function of state velocity vector $\{\overset{*}{q}\}$.

The nonlinear periodic response is obtained by solving Eq. (31) using quasilinearization,[15,16] which represents the solution by a sequence of linear response problems in an iterative manner. In this process the periodic solution of the linear system represented by Eq. (32)

$$\{\overset{*}{q}\}_{i+1} = [A(\psi;q_i)]\{q\}_{i+1} + \{F(\psi,q_i)\} \tag{32}$$

$$\{q(\psi=2\pi)\}_{i+1} = \{q(\psi=0)\}_{i+1} \tag{33}$$

is obtained using a technique similar to the one described in Ref. 16. However, the efficiency of this method was improved by avoiding the calculation of the inverse of the transition matrix.[12]

Once the nonlinear equilibrium position is obtained, the second part of the aeroelastic analysis consists of linearizing the equations of motion about the equilibrium condition by writing perturbation equations.[1,2] The stability of the linearized system is determined from Floquet theory.[2] The stability of the system is governed by the characteristic exponents $\lambda_k = \zeta_k + i\omega_k$, which are related to the eigenvalues of the transition matrix at the end of one period. When $\zeta_k > 0$, the system is unstable.

IV. Some Typical Results and Discussion

Two sets of results are calculated: 1) those which illustrate the influence of time-domain unsteady aerodynamics in hover and 2) those that show the influence of time-domain unsteady aerodynamics on the aeroelastic response and stability of a rotor blade in forward flight.

Uniform inflow was used in these calculations. For the case of hover, the inflow was evaluated from[10]

$$\lambda = (\sigma a_i/16)[\sqrt{1+(24\theta_G/\sigma a_i)} - 1] \tag{34}$$

while for forward flight it is calculated from[10]

$$\lambda = \mu\tan(\alpha_R) + C_T/2\sqrt{\mu^2+\lambda^2} \tag{35}$$

The effect of finite-state, arbitrary-motion, unsteady aerodynamics on a typical flap-lag stability boundary in hover, without elastic coupling ($R_c = 0$), is illustrated in Fig. 4. The results indicate that the differences between the two sets of curves, those based on quasisteady aerodynamics and those based on unsteady aerodynamics, are relatively small. An alternative means for showing the influence of unsteady aerodynamics is to plot the variation of the real part of the eigenvalues associated with flap and lag degrees of freedom as a function of the rotating lead-lag frequency $\bar{\omega}_{L1}$, as shown in Figs. 5 and 6. For each of these plots, the flap frequency is kept constant while the lag frequency is varied. In general, the results indicate that the two curves, representing lag damping, cross each other in the vicinity of $\bar{\omega}_{L1} = \bar{\omega}_{F1}$

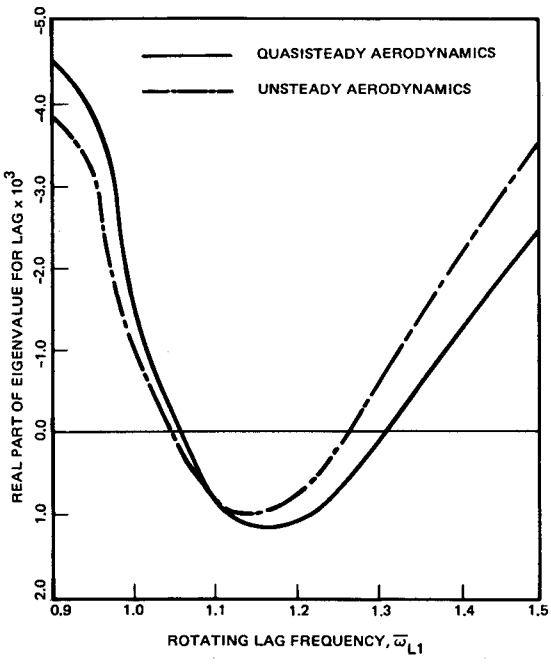

Fig. 5 Comparison of real part of lead-lag eigenvalue calculated using quasisteady and unsteady aerodynamics for $\bar{\omega}_{F1} = 1.1$. ($\theta_G = 0.25$, $R_c = 0.0$, $\gamma = 5.0$, $\sigma = 0.05$, $b = 0.01964$, $x_A = x_I = e = \beta_p = 0.0$, no apparent mass.)

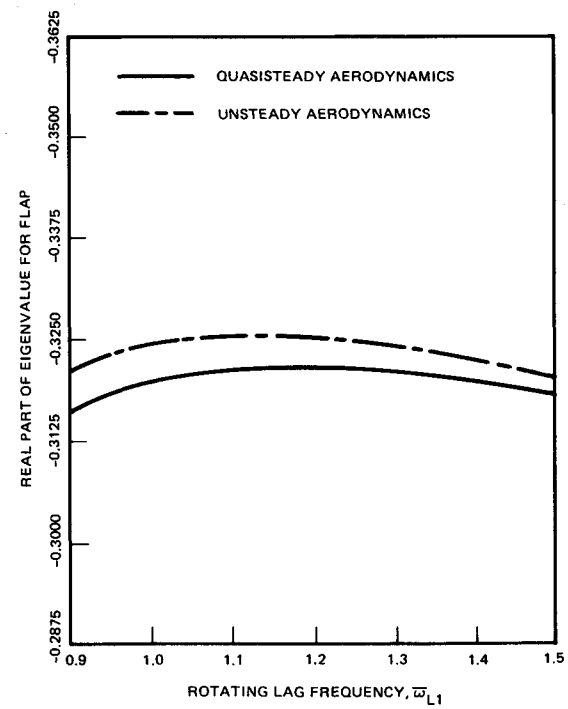

Fig. 6 Comparison of real part of eigenvalue for flap calculated using quasisteady and unsteady aerodynamics for $\bar{\omega}_{F1} = 1.1$. ($\theta_G = 0.25$, $R_c = 0.0$, $\gamma = 5.0$, $\sigma = 0.05$, $b = 0.01964$, no apparent mass.)

(Fig. 6). For $\bar{\omega}_{L1} < \bar{\omega}_{F1}$, the lead-lag damping with quasisteady aerodynamics is larger than the damping with arbitrary-motion unsteady aerodynamics. This trend is reversed when $\bar{\omega}_{L1} > \bar{\omega}_{F1}$. On the other hand, for the flap degree of freedom the damping with unsteady aerodynamics is always slightly higher for this particular case than that obtained with quasisteady aerodynamics. A considerable number of additional results for hover can be found in Ref. 12.

The results for forward flight are considered next. The blade configuration considered had the following properties:

$$\bar{\omega}_{F1} = 1.125,\ \bar{\omega}_{L1} = 0.732,\ \sigma = 0.07,\ \gamma = 5.5,$$

$$b = 0.0275,\ C_W = 0.005$$

Results for this configuration were obtained with three separate values of the elastic coupling parameter R_c, namely, $R_c = 0.0$, $R_c = 0.50$, and $R_c = 1.0$. In this paper, only the results for $R_c = 0.0$ are presented; additional results can be found in Ref. 12.

Blade response in the flap and lag degrees of freedom for $R_c = 0.0$ at an advance ratio of $\mu = 0.40$ is presented in Fig. 7, where the response over a revolution calculated using time-domain unsteady aerodynamics is compared with the response obtained using quasisteady aerodynamics. The influence of unsteady aerodynamics is much more pronounced for the flap response than it is for the lead-lag response. The effect of phase lag and amplitude modulation associated with the unsteady aerodynamics is also evident in Fig. 7. When the angle of attack is decreasing in time, the unsteady loads lag behind the angle of attack and thus the response with unsteady aerodynamics is higher than the response obtained using quasisteady aerodynamics. This situation occurs on the advancing blade in the vicinity of $\psi = 90$ deg, and it is reversed on the retreating blade.

The influence of unsteady aerodynamics on the blade stability is illustrated in Figs. 8 and 9 for $R_c = 0.0$, where the real parts of the characteristic exponents for the flap and lag degrees of freedom are plotted. It is important to emphasize that in a periodic system the real part of the characteristic exponent is only a measure of damping, and it is not the actual value of the damping. From Figs. 8 and 9 it is evident that use of time-domain unsteady aerodynamics reduces somewhat the damping in both the flap and lag degrees of freedom. An interesting aspect of the blade dynamics, in the presence of unsteady time-domain aerodynamics, is the instability in the flap degree of freedom that occurs at an advance ratio of $\mu = 0.45$, shown in Fig. 9. When quasisteady aerodynamics are used, this instability does not occur at all. To verify whether this instability is caused by the unsteady aerodynamics, the time-varying lift deficiency function has been calculated and plotted in Fig. 10 for three different values of the advance ratio specified in the figure. It should be noted that the time-domain lift deficiency function represents the ratio between the unsteady lift and the quasisteady lift. As evident from the figure, there is a rapid increase in the value of this function with advance ratio around $\psi = 90$ deg. Therefore, it is quite possible that the instability in the flap degree of freedom is caused by the unsteady aerodynamic loading.

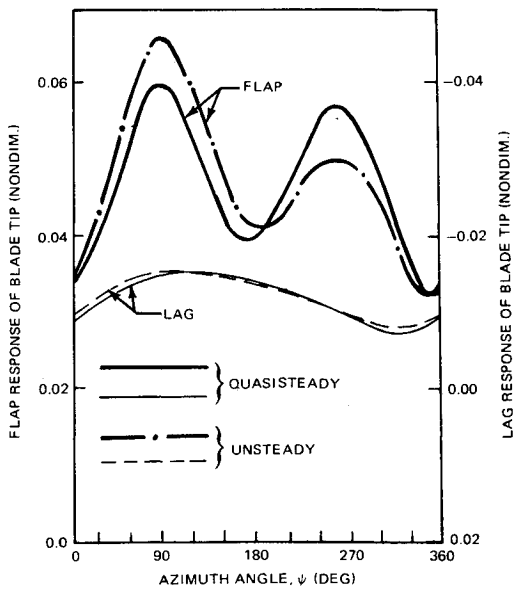

Fig. 7 Comparison of flap and lag response time histories calculated using quasisteady and unsteady aerodynamics for $\mu = 0.400$; propulsive trim; $R_c = 0.0$. (Quasilinearization; 4 iterations; 60 time steps/revolution.)

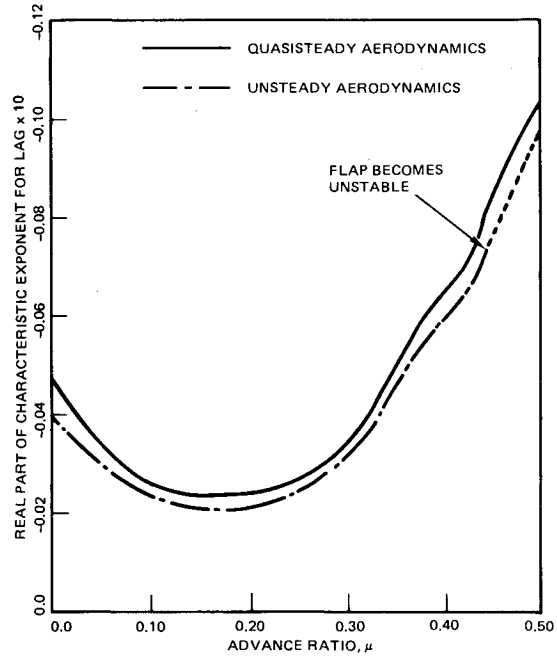

Fig. 8 Comparison of real part of characteristic exponent for lag, calculated using quasisteady and unsteady aerodynamics; propulsive trim; $R_c = 0.0$.

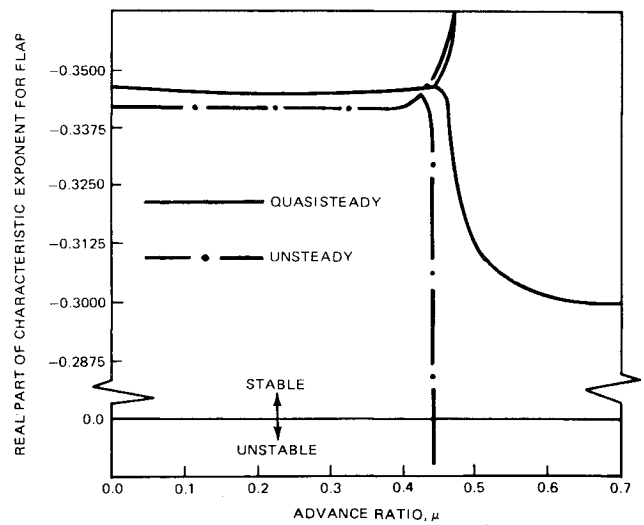

Fig. 9 Real part of characteristic exponent for flap calculated using quasisteady and unsteady aerodynamics; propulsive trim; $R_c = 0.0$.

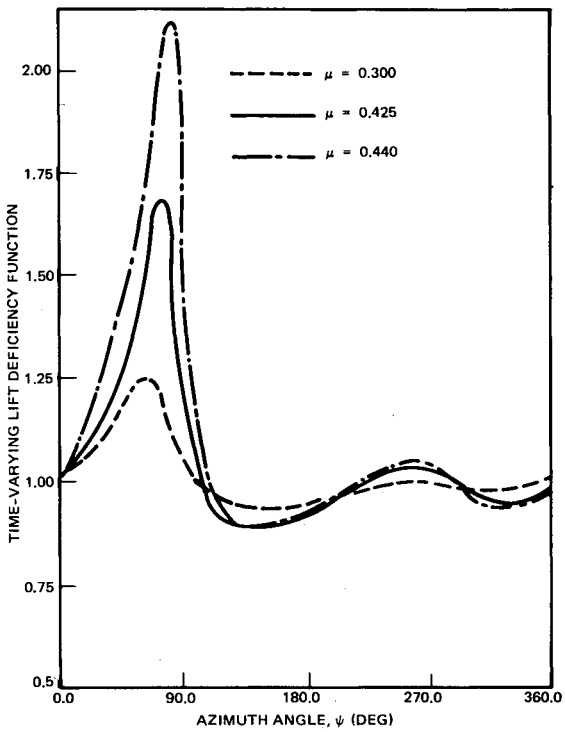

Fig. 10 Time-varying lift deficiency function with full blade dynamics at various advance ratios, $R_c = 0.0$.

The influence of unsteady aerodynamics on the blade stability with full elastic coupling, $R_c = 1.0$, was also studied in Ref. 12. For this particular case, elastic coupling does not remove the instability present in the flap degree of freedom. This behavior is reasonable since elastic coupling tends to stabilize primarily those instabilities associated with the lag degree of freedom. Numerous additional results can be found in Ref. 12.

V. Concluding Remarks

This paper presents for the first time the solution of a rotary-wing aeroelastic problem in hover and forward flight based on finite-state, time-domain, unsteady aerodynamics that is valid for arbitrary motions. For the case of hover, the influence of unsteady aerodynamics on the coupled flap-lag aeroelasticity stability boundaries is relatively minor. In forward flight, time-domain unsteady aerodynamics are quite important because, with this theory, it is possible to incorporate unsteady aerodynamics into the equations of blade motion in a manner consistent with the periodic coefficients present in these equations. On the other hand, frequency-domain unsteady aerodynamics cannot be conveniently incorporated into equations of motion that have periodic coefficients.

The numerical results indicate that flap response and flap stability are items that are primarily influenced by unsteady aerodynamics. At high advance ratios, a flap instability can be caused by unsteady aerodynamic effects. It should be noted however, that at such high advance ratios the influence of compressibility and dynamic stall,[1] which was neglected in this study, could significantly influence the results.

Finally, it should be noted that the unsteady aerodynamic theory described in this paper is particularly applicable to rotary-wing aeroelastic problems in which the blade motion is represented by fully coupled flap-lag-torsional dynamics or in which there is coupling with an active control system.

Acknowledgment

This work was supported by NASA Ames Research Center under Grant NASA NAG 2-209.

References

[1]Friedmann, P. P., "Formulation and Solution of Rotary-Wing Aeroelastic Stability and Response Problems," *Vertica*, Vol. 7, No. 2, 1983, pp. 101-141.

[2]Friedmann, P. P., "Recent Developments in Rotary-Wing Aeroelasticity," *Journal of Aircraft*, Vol. 14, Nov. 1977, pp. 1027-1041.

[3]Dinyavari, M.A.H. and Friedmann, P. P., "Unsteady Aerodynamics in Time and Frequency Domains for Finite Time Arbitrary Motion of Rotary Wings in Hover and in Forward Flight," *Proceedings AIAA/ASME/ASCE/AHS 25th Structures, Structural Dynamics and Materials Conference*, Palm Springs, CA, May 1984, pp. 266-282.

[4]Greenberg, J. M., "Airfoil in Sinusoidal Motion in Pulsating Stream," NACA TN 1326, 1947.

[5]Loewy, R. G., "A Two-Dimensional Approximation to the Unsteady Aerodynamics of Rotary Wings," *Journal of the Aeronautical Sciences*, Vol. 24, Feb. 1957, pp. 81-92, 144.

[6]Ormiston, R. A. and Hodges, D. H., "Linear Flap-Lag Dynamics of Hingeless Helicopter Rotor Blades in Hover," *Journal of the American Helicopter Society*, Vol. 17, April 1972, pp. 2-14.

[7]Peters, D. A., "Flap-Lag Stability of Helicopter Rotor Blades in Forward Flight," *Journal of the American Helicopter Society*, Vol. 20, Oct. 1975, pp. 2-13.

[8]Peters, D. A. and Gaonkar, G. H., "Theoretical Flap-Lag Damping with Various Dynamic Inflow Models," *Journal of the American Helicopter Society*, Vol. 25, July 1980, pp. 29-36.

[9]Gaonkar, G. H. and Peters, D. A., "Use of Multiblade Coordinates for Helicopter Flap Stability with Dynamic Inflow," *Journal of Aircraft*, Vol. 17, Feb. 1980, pp. 112-118.

[10]Johnson, W., *Helicopter Theory*, Princeton University Press, Princeton, NJ, 1980.

[11]Edwards, J. W., "Unsteady Aerodynamics Modeling and Active Aeroelastic Control," Guidance and Control Laboratory, Department of Aeronautics and Astronautics, Stanford University, Stanford, CA, SUDAAR 504, Feb. 1977.

[12]Asghar-Hessari-Dinyavari, M., "Unsteady Aerodynamics in Time and Frequency Domains for Finite-Time Arbitrary-Motion of Helicopter Rotor Blades in Hover and Forward Flight," Ph.D. Dissertation, Mechanical, Aerospace and Nuclear Engineering Department, University of California, Los Angeles, CA, March 1985.

[13]Venkatesan, C. and Friedmann, P. P., "Aeroelastic Effects in Multi-Rotor Vehicles with Applications to a Hybrid Heavy Lift System, Part I: Formulation of Equations of Motion," NASA CR-3822, Aug. 1984.

[14]Venkatesan, C. and Friedmann, P. P., "Finite State Modeling of Unsteady Aerodynamics and Its Application to a Rotor Dynamic Problem," School of Engineering and Applied Science, University of California, Los Angeles, Rept. UCLA-ENG-85-10, March 1985.

[15]Friedmann, P. P. and Kottapalli, S.B.R., "Rotor Blade Aeroelastic Stability and Response in Foward Flight," Paper no. 14, *Proceedings of the 6th European Rotorcraft Forum*, Bristol, England, Sept. 1980.

[16]Friedmann, P. P. and Kottapalli, S.B.R., "Coupled Flap-Lag-Torsional Dynamics of Hingeless Rotor Blades in Forward Flight," *Journal of the American Helicopter Society*, Vol. 27, Oct. 1982, pp. 28-36.